

Geophysical Research Letters

RESEARCH LETTER

10.1029/2019GL082136

Key Points:

- Shipborne GNSS PWV retrieval is demonstrated with an accuracy of 1 mm, and an agreement of 1.7 mm with satellite altimetry PWV
- The multi-GNSS solution shows an RMS improvement of ~10% compared to the GPS solution in oceanwide PWV retrieval using kinematic PPP method
- Shipborne GNSS PWV retrieval could expand GNSS meteorology to ocean and improve NWM, satellite altimetry, and weather forecasting

Supporting Information:

- Supporting Information S1

Correspondence to:

Z. Wu,
wuzhilu@hhu.edu.cn

Citation:

Wang, J., Wu, Z., Semmling, M., Zus, F., Gerland, S., Ramatschi, M., et al. (2019). Retrieving precipitable water vapor from shipborne multi-GNSS observations. *Geophysical Research Letters*, 46, 5000–5008. <https://doi.org/10.1029/2019GL082136>

Received 10 DEC 2018

Accepted 20 APR 2019

Published online 15 MAY 2019

Retrieving Precipitable Water Vapor From Shipborne Multi-GNSS Observations

Jungang Wang^{1,2} , Zhilu Wu^{1,3} , Maximilian Semmling¹ , Florian Zus¹ , Sebastian Gerland⁴ , Markus Ramatschi¹, Maorong Ge¹ , Jens Wickert^{1,2} , and Harald Schuh^{1,2} 

¹Department of Geodesy, GeoForschungsZentrum (GFZ), Potsdam, Germany, ²Institute of Geodesy and Geoinformation Science, Technische Universität Berlin, Berlin, Germany, ³College of Earth Science and Engineering, Hohai University, Nanjing, China, ⁴Norwegian Polar Institute, Fram Centre, Tromsø, Norway

Abstract Precipitable water vapor (PWV) is an important parameter for climate research and a crucial factor to achieve high accuracy in satellite geodesy and satellite altimetry. Currently Global Navigation Satellite System (GNSS) PWV retrieval using static Precise Point Positioning is limited to ground stations. We demonstrated the PWV retrieval using kinematic Precise Point Positioning method with shipborne GNSS observations during a 20-day experiment in 2016 in Fram Strait, the region of the Arctic Ocean between Greenland and Svalbard. The shipborne GNSS PWV shows an agreement of ~1.1 mm with numerical weather model data and radiosonde observations, and a root-mean-square of ~1.7 mm compared to Satellite with ARGOS and ALTiKa PWV. An improvement of 10% is demonstrated with the multi-GNSS compared to the Global Positioning System solution. The PWV retrieval was conducted under different sea state from calm water up to gale. Such shipborne GNSS PWV has the promising potential to improve numerical weather forecasts and satellite altimetry.

Plain Language Summary Atmospheric water vapor retrieval using GNSS kinematic Precise Point Positioning technique is demonstrated with shipborne GNSS data collected during a 20-day cruise in Fram Strait (~80°N), the area in the Arctic Ocean between Greenland and Svalbard. An accuracy of ~1 mm is achieved compared to ERA-Interim precipitable water vapor (PWV) and radiosonde data, and an agreement of ~2 mm is demonstrated between shipborne GNSS PWV and satellite altimetry PWV observation. The contribution of multi-GNSS is addressed, and efforts are also made to investigate the PWV spatial resolution in order to include more data for comparison. Static Precise Point Positioning method is widely used at ground-based GNSS stations in climate research and weather forecasting. However, it is still limited to land. Shipborne GNSS PWV retrieval could fill in the vast ocean with high temporal/spatial resolutions. Shipborne GNSS PWV could cover open sea, coastal, and polar regions (e.g., in this study) where regular meteorological observations are rare. Shipborne GNSS PWV retrieval in real time is feasible and could provide additional information for weather predictions. Moreover, shipborne GNSS PWV retrieval provides a potential method for satellite altimetry calibration, the major technique measuring sea surface height for sea level monitoring.

1. Introduction

Atmospheric water vapor is an important parameter for the climate research (Alshawaf et al., 2018; Balidakis et al., 2018) and a valuable input for numerical weather model (NWM; Gutman et al., 2004; Oigawa et al., 2018). Retrieving precipitable water vapor (PWV) using Global Navigation Satellite System (GNSS) with 1- to 2-mm accuracy has been demonstrated at ground-based stations (Wang et al., 2007). Static Precise Point Positioning (PPP) method is widely used due to its efficiency and high precision (Byun & Bar-Sever, 2009), and an improved solution is achieved by multi-GNSS (Li et al., 2015). PWV from coastal ground-based GNSS stations has also been used to improve satellite altimetry (Brown, 2010; Fernandes et al., 2010; Fernandes et al., 2015). However, static PPP could only be used at ground-based stationary GNSS stations over land, which is a large limitation. GNSS PWV retrieval from oceanwide platforms can expand GNSS meteorology to the vast ocean and has broad applications in NWM assimilation, satellite altimetry, and weather forecasting.

PWV retrieval from a moving platform is challenging due to the simultaneous estimation of the epoch-wise antenna coordinates and the troposphere delay. It is more difficult in ocean due to the large multipath effect

from the water surface and sea ice and the potential rough sea condition caused by large wind. PWV retrieval using relative positioning method was demonstrated with an accuracy of 1–3 mm (Cardellach et al., 2000; Chadwell & Bock, 2001; Dodson et al., 2001), but relative positioning is limited to coastal regions. Kinematic PPP method does not rely on reference stations and is more suitable in open sea. Using kinematic PPP Rocken et al. (2005) achieved the open-sea Global Positioning System (GPS) PWV retrieval of 1.5–2 mm with respect to (w.r.t.) radiosonde and 2.8 mm w.r.t. Water Vapor Radiometer (WVR); Fujita et al. (2008) demonstrated a GPS PWV agreement of ~ 2.3 mm with ~ 300 radiosonde profiles in equatorial ocean. Kealy et al. (2012) presented the use of GPS PWV for identifying atmosphere synoptic and mesoscale features; Boniface et al. (2012) investigated the difference between GPS PWV and NWM PWV in the Mediterranean Sea and attributed the large offsets to the NWM's excursions during the transition between local weather conditions.

This study investigates the use of shipborne GNSS observations for PWV retrieval during a 20-day experiment in Fram Strait between Greenland and Svalbard, the gateway to the Arctic Ocean, where the warm water flows northward from the Atlantic Ocean and the sea ice leaves the Arctic Ocean. This study is different from the aforementioned ones in the following significant ways: (1) We present a throughout comparison of the oceanwide zenith tropospheric delay (ZTD) and PWV retrieval using kinematic PPP, including nearby ground-based GNSS and radiosonde stations, NWM, and Satellite with ARGOS and ALtiKa (SARAL) PWV, and the last one is unique compared to other studies and important for further satellite altimetry calibration; (2) the benefit of multi-GNSS in oceanwide PWV retrieval is addressed; (3) the temporal correlation is investigated to expand the service range of shipborne GNSS PWV; and (4) Fram Strait is of great interest for climate research, but poorly observed by satellite altimetry due to ice coverage, and the observations are contaminated by ice. Also, in this study the ship went through different sea conditions from calm water (covered by ice) up to gale (~ 20 -m/s wind); thus, it is more representative.

2. Data and Method

2.1. Shipborne GNSS Observation and Processing

The *R/V Lance* is used by the Norwegian Polar Institute for regular monitoring and research related to ocean and sea ice properties in Fram Strait (de Steur et al., 2014, 2018; Renner et al., 2014). During the Fram Strait 2016 cruise from day-of-year (DOY) 238 to DOY 257, a GNSS reflectometry (GNSS-R) setup was installed aboard *R/V Lance* for the investigation of sea ice (Semmling et al., 2017), meanwhile a geodetic JAVAD TR_G3TH GNSS receiver was installed on the ship bow, which is about 6 m above water surface. This receiver collected multi-GNSS data at a sampling of 1 Hz, including GPS, GLONASS, and Galileo.

The Positioning And Navigation system Data Analyst (Liu & Ge, 2003; Penna et al., 2018) was used to conduct a GPS + GLONASS + Galileo combined kinematic PPP solution (hereinafter referred to as GRE PPP), where epoch-wise antenna coordinates and ZTD were estimated simultaneously with other parameters. The hydrostatic delay was derived with the Global Pressure and Temperature (GPT) model (Boehm et al., 2007) using Saastamoinen equation (Saastamoinen, 1972), while the wet delay was estimated as random walk noise with a process noise of $4 \text{ mm}/\sqrt{h}$, and the Global Mapping Function (Boehm et al., 2006) was used. The 1-Hz observations were resampled to 30 s, and the forward and backward method was applied to avoid the ambiguity convergence problem. The ionosphere-free combined observations were used with an elevation cutoff of 7° . The GRM final product (Loyer et al., 2016) from Centre National d'Etudes Spatiales/Collecte Localisation Satellites were fixed in the PPP. Besides the GRE PPP, we also conducted the GPS-only PPP solution (hereinafter referred to as GPS PPP) to demonstrate the contribution of the multi-GNSS solution. The usable satellite number per epoch for PPP is shown in Figure 1b. On average 9.62 satellites can be used per epoch for GPS PPP, while the number is doubled for GRE PPP.

As shown in Figure 1a, the ship started on DOY 238 from Svalbard and arrived at Greenland on DOY 248. Then it started to go back and returned to the launch location on DOY 257. During the cruise the ship went through different sea states, with wind speed up to ~ 20 m/s and ship heave up to ± 2 m. The ship either stopped for scientific experiment or went at an average speed of ~ 4 m/s (see results in Figure S1 in the supporting information).

The shipborne GNSS PWV was derived from the ZTD estimates, where zenith hydrostatic delay (ZHD) and weighted mean temperature T_m were computed from the European Centre for Medium-Range Weather

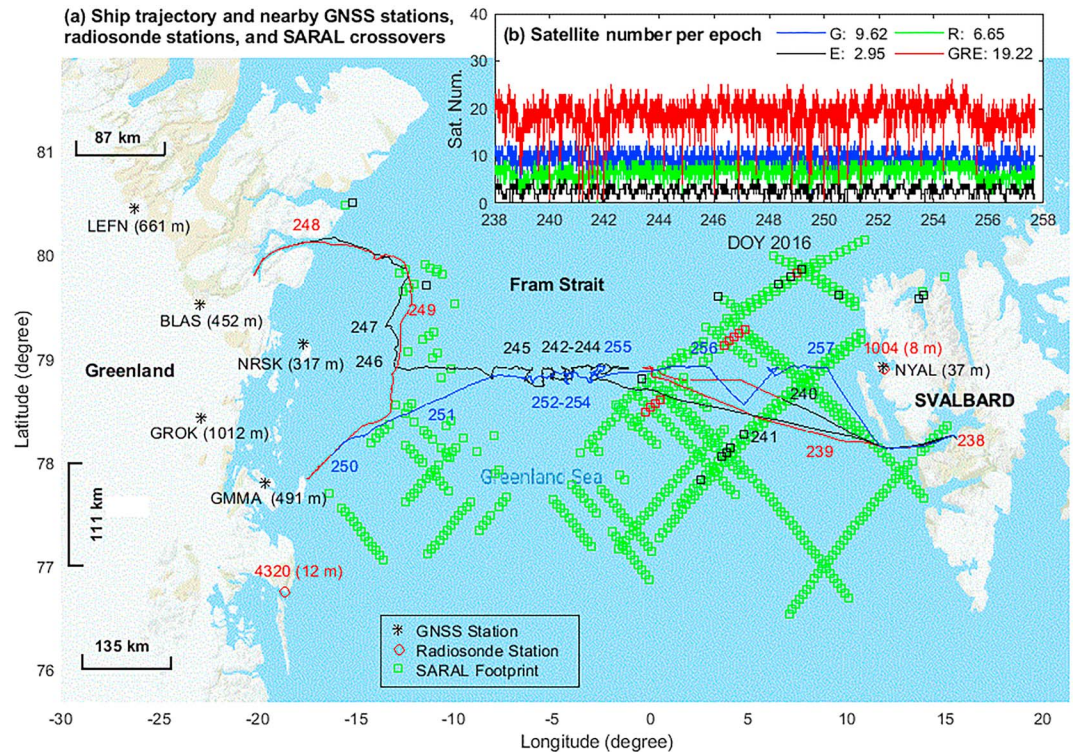


Figure 1. (a) Ship trajectory from start at (78.23°N, 15.63°E) on DOY 238 to the end on DOY 257 at the same location, with the distribution of ground reference GNSS stations (black star), radiosonde stations on land (red circle), and SARAL crossovers within 200 km in 2 hr (rectangles in green, red and black); (b) usable satellite number per epoch for GPS PPP (G, blue line) and GRE PPP (GRE, red line), where the numbers of GLONASS (R, green line) and Galileo (E, black line) are also specified. In panel (a) the height above mean sea level (MSL) is presented for all the GNSS and radiosonde stations. The SARAL crossovers in green are valid observations, and that in red are outliers with negative values; those in black are outliers detected with the linear fit using precipitable water vapor of shipborne GRE PPP. The distance scale is different at this location; thus, we show that on both latitude and longitude scales. GNSS = Global Navigation Satellite System; SARAL = Satellite with ARGOS and ALtiKa; DOY = day-of-year; GPS = Global Positioning System; PPP = Precise Point Positioning.

Forecasts (ECMWF) ERA-Interim pressure level data (Berrisford et al., 2011; Bevis et al., 1994; Zus et al., 2012). The calculation of ZHD and T_m will be discussed in section 2.3.

2.2. ZTD at Ground GNSS Stations

As shown in Figure 1a, six nearby ground GNSS stations were used for the validation of shipborne ZTD in coastal areas, including the International GNSS Service (IGS) station NYAL and five stations from the University NAVSTAR Consortium POLENET Greenland Network. The ZTD estimates were derived in static PPP mode for the same period using the similar setting as for the shipborne PPP solution, except that in static PPP receiver coordinates were estimated as daily constant. For the station NYAL kinematic PPP was also conducted, and the root-mean-square (RMS) compared to the IGS final ZTD product (Byun & Bar-Sever, 2009) were 0.40 and 0.34 cm for kinematic and static solutions, respectively. However, the ZTD error from shipborne GNSS PPP is usually greater due to the ship motion and the multipath effects.

As the maximum elevation of the reference stations is greater than 1 km, the ZTD height correction is applied before comparing to the shipborne ZTD at an elevation of 6 m. An exponential decay function was used to model the ZTD variation w.r.t. elevation:

$$ZTD_h = ZTD_0 \times e^{-\frac{h}{H}} \quad (1)$$

where ZTD_0 and ZTD_h are the zenith total delays at mean sea level and station elevation, respectively; h is the station elevation. Using the 20-day ZTD estimates of the five stations on Greenland, the ZTD scale height H was estimated to be 7.94 km. Then the ZTD at the elevation of 6 m was derived with this height correction

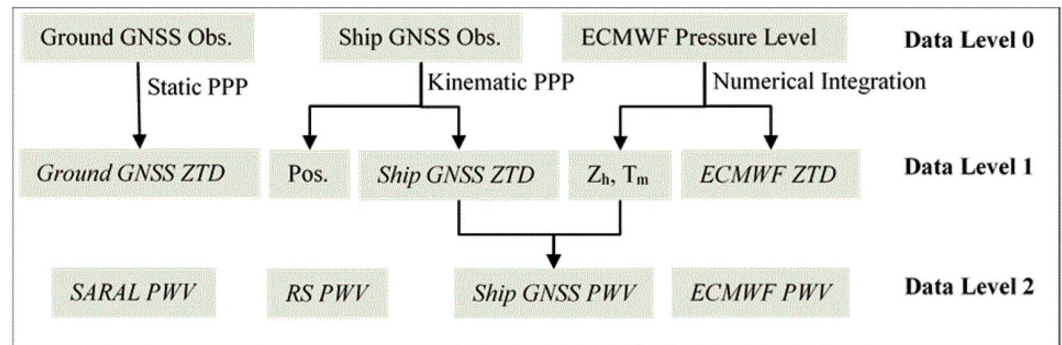


Figure 2. Data processing sequence for shipborne GNSS ZTD/PWV comparison. GNSS = Global Navigation Satellite System; ECMWF = European Centre for Medium-Range Weather Forecasts; ZTD = zenith tropospheric delay; SARAL = Satellite with ARgos and ALtiKa; PWV = precipitable water vapor.

method. Figure 3c shows the interstation ZTD comparison of the five stations on Greenland. The ZTD RMS is 0.5–0.9 cm within 200 km, and always less than 1.1-cm even at 320 km.

2.3. ECMWF Product

The ERA-Interim pressure level data were used to calculate the ZTD, ZHD, and T_m on the ship trajectory. The 6-hr sampled $0.125^\circ \times 0.125^\circ$ grid data were linearly and bilinearly interpolated temporally and spatially to obtain the corresponding values at the 30-s sampled ship track. The ZHD and T_m were used for the derivation of GNSS PWV from the shipborne GNSS ZTD (Wang et al., 2005).

In addition to the ECMWF ZTD, the integrated water vapor from ERA-Interim surface product was also used for the validation of shipborne GNSS PWV. The same interpolation method was applied to derive the PWV on the ship track.

2.4. Radiosonde Profile

Two radiosonde stations were used for the PWV validation, which are shown in Figure 1a. The station 1004 (identifier: ENAS) in Ny-Alesund has one observation per day at 12:00 UTC. The other station 4320 (identifier: BGDH) located in Greenland has two observations per day at 00:00 and 12:00 UTC. Since the daily radiosonde observation number is low and the ship can be far away from these stations, the spatial and temporal overlap for comparison with radiosonde profiles is small.

2.5. Spaceborne Observation

The SARAL is a joint satellite mission of the Indian Space Research Organization and Centre National d'Etudes Spatiales. Designed to realize precise, repetitive global measurements of sea surface height, significant wave heights, and wind speed, SARAL payload integrates a high-resolution single frequency ALtiKa altimeter (Ka-band) that includes a dual frequency radiometer function shared on a common antenna. The two-band radiometer (23.8 and 37 GHz) is used onboard to sense PWV. The 98.538° inclined SARAL orbit has a global coverage including the polar areas and the ship track (Mahesh Kumar et al., 2015; Picard et al., 2015; Verron et al., 2015).

The crossover between ship trajectory and SARAL is defined as a SARAL footprint of less than 200 km to the ship in 2 hr, which is shown in Figure 1a. All the footprints not marked as “ocean” or flagged as “ice covered” were excluded. Among the rest, those with negative PWV values were also excluded as outliers, which contributes to ~1.6%.

2.6. Data Comparison Method

The aforementioned data sources are summarized in Figure 2. Shipborne ZTD was first compared with ground GNSS stations, and at each station all the shipborne ZTD within 200 km was used. The ECMWF products were then used to assess the shipborne ZTD/PWV along the ship track. Shipborne PWV was further compared with radiosonde profiles and SARAL PWV observations.

As more observations are available within greater distance, the ZTD/PWV spatial correlation decreases with the increase of distance. Thus, we use different distance criteria when compared with ground GNSS stations

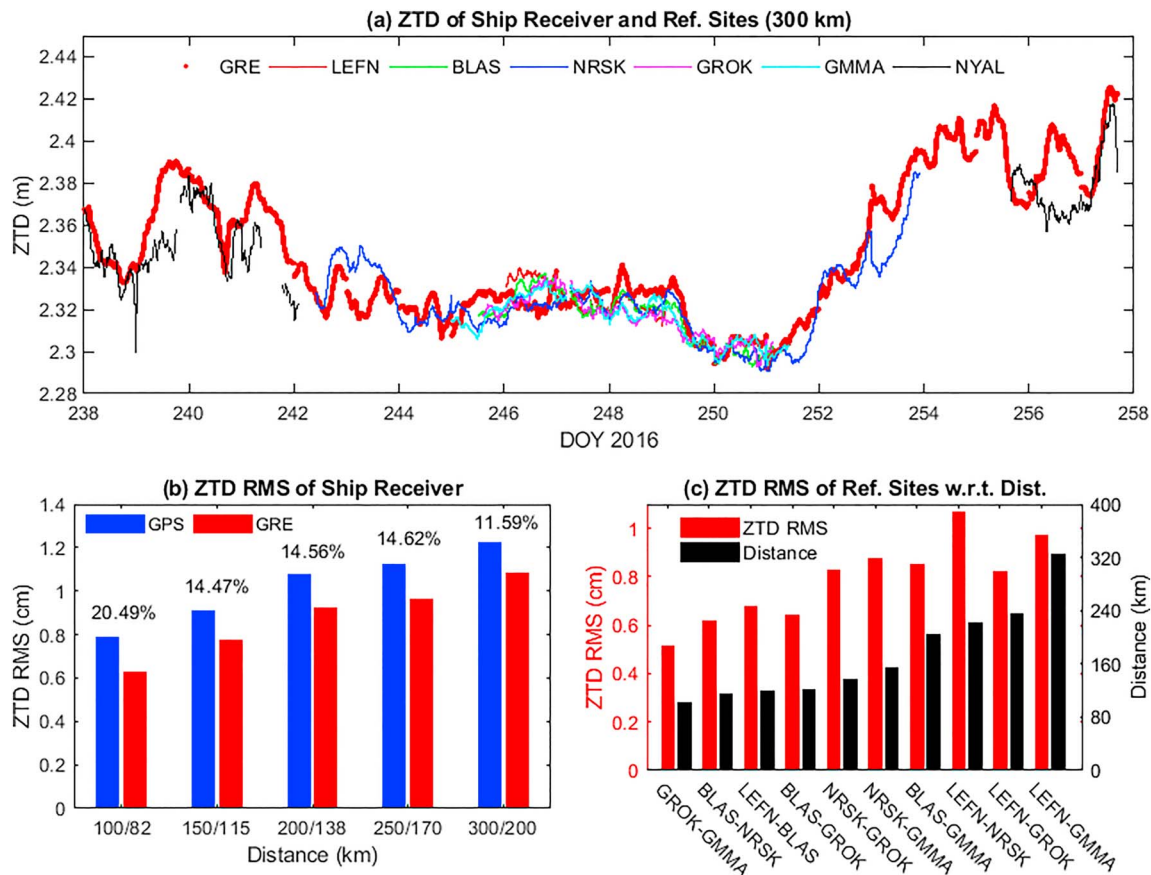


Figure 3. (a) ZTD of shipborne GRE PPP (red dots) and ground GNSS stations within 300 km; (b) ZTD RMS of GPS PPP (blue) and GRE PPP (red) with respect to ground stations within different distances; (c) interstation ZTD comparison after height correction and the inter-station distance. In panel (b) the X-label is the maximum and average distances, and the improvement of GRE solution compared to GPS solution is labeled above each column. ZTD = zenith tropospheric delay; PPP = Precise Point Positioning; GNSS = Global Navigation Satellite System; RMS = root-mean-square; DOY = day-of-year.

and SARAL observations, that is, 100–300 and 50–200 km, respectively, with an interval of 50 km. The temporal resolution for comparison was set as 2 hr. The shipborne GNSS PWV comparison with ECMWF and SARAL data was done with the direct difference and then using the linear fit, and observations with a difference greater than 3 times of the RMS were excluded; that is, the 3σ rule was applied.

3. Results and Discussions

3.1. ZTD Comparison With Reference GNSS Stations

The ZTD estimates from both GPS PPP and GRE PPP are shown in Figure 3a, together with the ZTD values of reference stations within 300 km from the ship. The RMS values of shipborne GNSS ZTD compared to ground stations within different distance criteria are shown in Figure 3b, and the interstation comparison of ground GNSS ZTD is shown in Figure 3c.

As shown in Figure 3, shipborne GNSS ZTD agrees well with that at the reference station. The RMS of GPS PPP and GRE PPP is 0.78 and 0.62 cm within 100 km (average: 82 km). Within 300 km (average: 200 km) the RMS values for GPS PPP is 1.22 cm and that for GRE PPP is 1.08 cm. Compared to GPS PPP, ZTD from GRE PPP is improved by ~10% within 300 km and ~20% within 100 km. Also, with more observations for comparison at a greater distance, the RMS increases due to the less spatial correlation of ZTD in a greater area. The relative large RMS of shipborne GNSS ZTD compared to that at the NYAL station, that is, 0.34/0.40 cm for static/kinematic PPP, could be caused by the ship-ground station distance, the height correction approximation, and the rough sea state. The large ZTD discrepancy between shipborne GNSS and NYAL on DOY 256 was caused by the large water vapor gradient (see results in Figure S2 in the supporting information).

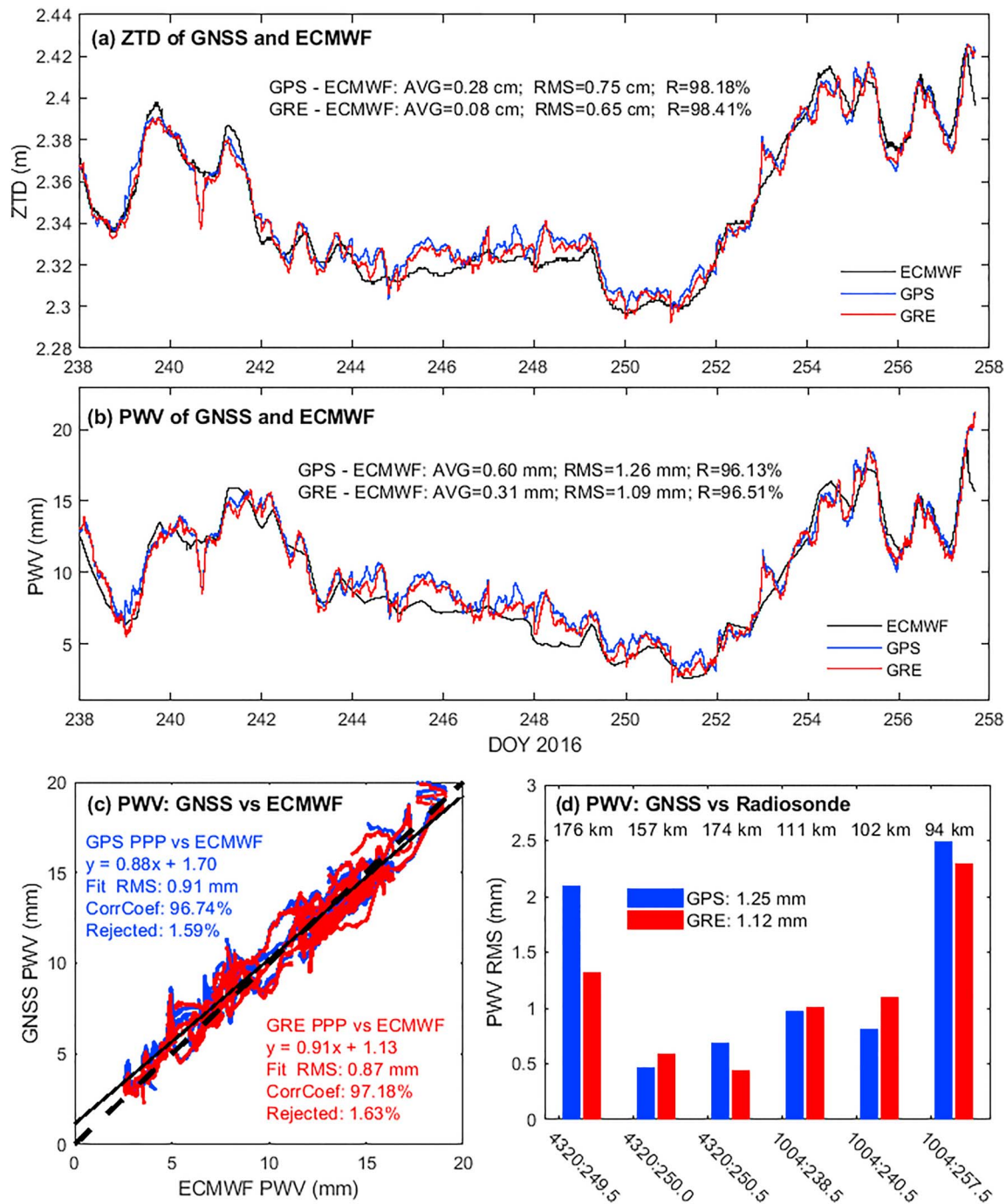


Figure 4. (a) ZTD and (b) PWV of ECMWF (black line), shipborne GPS PPP (blue line), and shipborne GRE PPP (red line); (c) PWV linear correlation between ECMWF and GPS PPP (in blue), ECMWF and GRE PPP (in red) and the corresponding statistics; (d) PWV RMS of GPS PPP (blue) and GRE PPP (red) compared to radiosonde data. In panel (c) the black solid line is the fit result of ECMWF and GRE PPP, and the black dashed line is the reference of $y = x$. ZTD = zenith tropospheric delay; GNSS = Global Navigation Satellite System; ECMWF = European Centre for Medium-Range Weather Forecasts; RMS = root-mean-square; GPS = Global Positioning System; PWV = precipitable water vapor.

3.2. PWV Comparison With ERA-Interim and Radiosonde

The ZTD values of ECMWF and shipborne GNSS are shown in Figure 4a. The GNSS ZTD shows a good agreement with the ECMWF ZTD, with a correlation coefficient of 98.2% for GPS PPP and that of 98.4% for GRE PPP. The average bias between GPS PPP and ECMWF is 0.28 cm, and the RMS value is 0.75 cm.

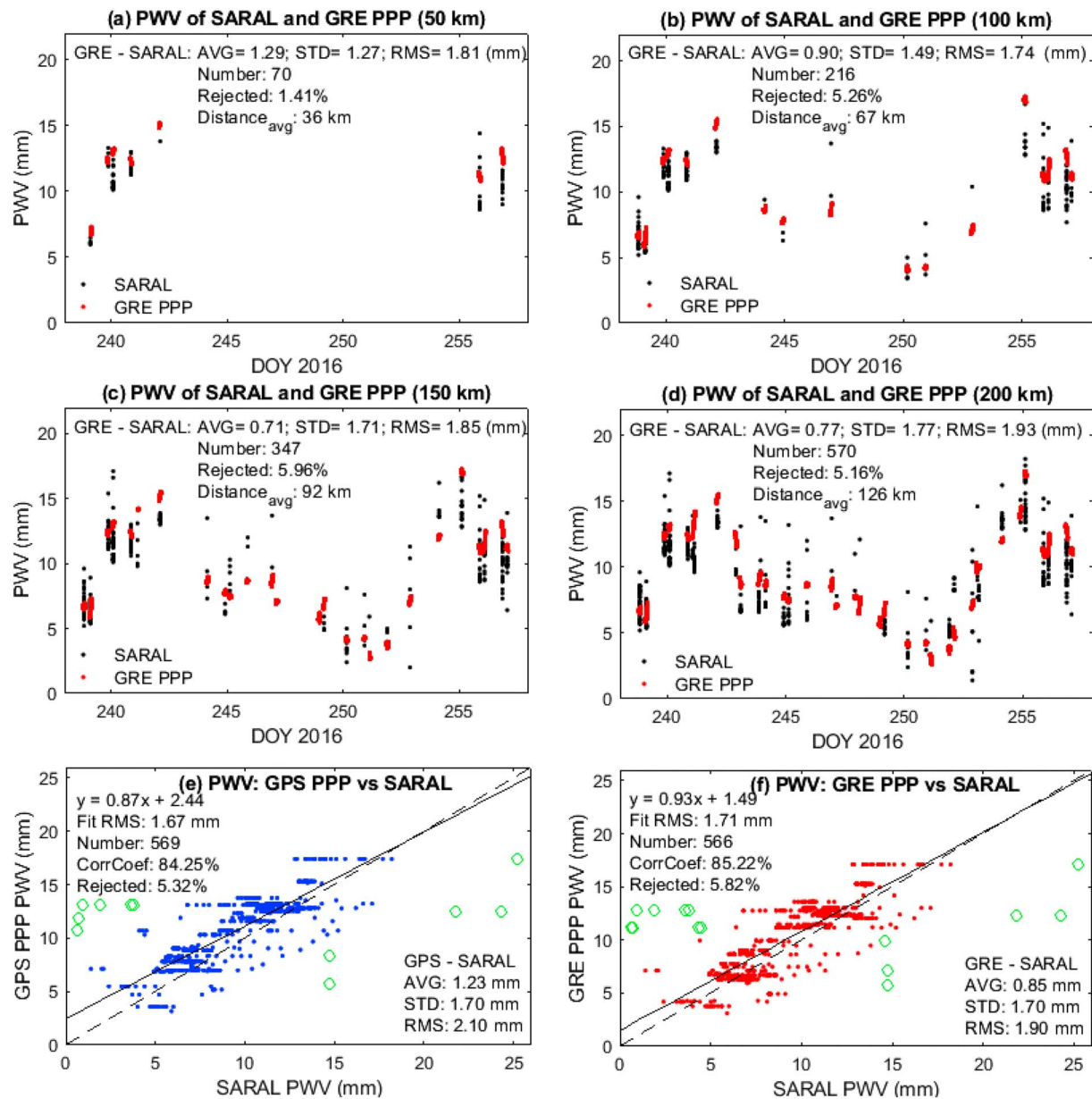


Figure 5. PWV of SARAL (black dot) and GRE PPP (red dot) within: (a) 50 km, (b) 100 km, (c) 150 km, and (d) 200 km. PWV linear correlation between SARAL and GNSS for (e) GPS PPP, and (f) GRE PPP, within 200 km. In panels (e) and (f) the outliers are shown in green circles; the statistic of the linear fit is shown in left top and the statistic of the direct comparison is shown in bottom right. PWV = precipitable water vapor; SARAL = Satellite with ARGOS and ALtiKa; PPP Precise Point Positioning; RMS = root-mean-square; DOY = day-of-year.

Compared with GPS PPP, GRE PPP shows an improvement of ~13%, with an average bias of 0.08 cm and RMS of 0.65 cm.

The PWV comparison between the ERA-Interim surface product and shipborne GNSS PPP solutions is shown in Figures 4b and 4c. PWV from GPS PPP is about 0.60 mm greater than that of ECMWF, and this systematic bias is reduced to 0.31 mm for GRE PPP. The PWV RMS of GRE PPP (1.09 mm) shows an improvement of 13.5% compared to that of GPS PPP (1.26 mm). The systematic bias between ECMWF PWV and GNSS PWV is also demonstrated in the linear fit result, where the fit slope of GPS PPP is 0.88, while that for GRE PPP is 0.91. The fit RMS of GRE PPP (0.87 mm) is slightly better (4.4%) than that of GPS PPP. The ZTD/PWV discrepancy between shipborne GNSS and NWM is expected to be caused by the NWM error, as the shipborne result agrees well with the nearby ground stations (see Figure 3a).

Figure 4d shows the PWV comparison between shipborne GNSS and radiosonde profiles, where it can be seen that the GRE PPP achieves an RMS of 1.12 mm, indicating an improvement of 10.4% compared to the 1.25-mm RMS of GPS PPP. The distance between the radiosonde stations and the ship varies from 94 to 176 km, with an average value of 136 km.

3.3. PWV Comparison With SARAL Observations

Figures 5a–5d show the PWV of SARAL and GRE PPP within different distances from 50 to 200 km. In general, about 5% of the observations are rejected according to the 3σ rule, and 570 crossovers are available within 200 km with an average distance of 126 km. The PWV RMS between SARAL and GRE PPP is about 1.7–1.9 mm, while the GNSS PWV is about 0.7–0.9 mm greater than that of SARAL.

Figures 5e and 5f show the linear correlations between GNSS PWV and SARAL PWV within 200 km. Even though the 1.71-mm fit RMS of GRE PPP is greater than the GPS PPP, that is, 1.67 mm, the 0.04-mm difference (~2%) is insignificant. Compared to GPS PPP PWV, GRE PPP PWV shows a greater correlation (85.2% vs. 84.3%), a less RMS (1.90 vs. 2.10 mm), and a less bias (0.85 vs. 1.23 mm). In general, about 5% of the observations are excluded as outliers via the linear fit.

Though a good agreement of ~2 mm is demonstrated between SARAL PWV and shipborne GNSS PWV, the comparison reveals a systematic bias, where GNSS PWV is about 0.7–0.9 mm greater. Moreover, except for the PWV outliers with negative values excluded before the comparison, ~5% of the SARAL crossovers are detected as outliers. Therefore, it is expected that the shipborne GNSS PWV can help in validating and calibrating satellite altimetry PWV.

4. Conclusions

In this paper, we retrieved PWV from shipborne GNSS observations using the kinematic PPP technique. This technique does not depend on ground reference stations and provides very precise PWV (~1 mm in this study) with high temporal and spatial resolution and works perfectly in the ocean regions. A ZTD agreement of ~0.6 cm was achieved compared to ground GNSS stations and NWM, and the PWV agreement was about 1.1 mm compared to NWM and radiosonde profiles, which is better than the previous studies. Furthermore, compared with about 570 SARAL crossovers, the shipborne GNSS PWV shows good agreement with an RMS of about 2 mm, with ~5% SARAL observations detected as outliers. The benefit of the multi-GNSS solution was demonstrated with an improvement of 10% compared to GPS-only solution, as with multi-GNSS more satellites are available and the geometry is improved. The spatial correlation of ZTD/PWV was investigated to include more observations, which is important for the validation and calibration of satellite altimetry.

As the atmosphere sounding in the open-sea area is not as convenient as that on land where ground GNSS receivers and radiosonde stations are widely installed, shipborne GNSS technique could be a potential method to retrieve the PWV for weather forecasting. Shipborne GNSS PWV in coastal and polar regions is important for satellite altimetry due to the land and ice contamination problem of the altimetry PWV, and in open sea it also serves as an external source for the validation and calibration. Per day ~160,000 vessels are tracked by the Automatic Identification System (<https://www.marinetraffic.com>) and transmit signals via it; thus, using these shipborne GNSS PWV would have broad applications and significant improvement for atmosphere research. It is also expected to apply this method in real-time to provide additional information for numerical weather prediction.

References

- Alshawaf, F., Zus, F., Balidakis, K., Deng, Z., Hoseini, M., Dick, G., & Wickert, J. (2018). On the statistical significance of climatic trends estimated from GPS tropospheric time series. *Journal of Geophysical Research: Atmospheres*, 123, 10,967–10,990. <https://doi.org/10.1029/2018JD028703>
- Balidakis, K., Nilsson, T., Zus, F., Glaser, S., Heinkelmann, R., Deng, Z. G., & Schuh, H. (2018). Estimating integrated water vapor trends from VLBI, GPS, and numerical weather models: Sensitivity to tropospheric parameterization. *Journal of Geophysical Research: Atmospheres*, 123, 6356–6372. <https://doi.org/10.1029/2017JD028049>
- Berrisford, P., Dee, D. P., Poli, P., Brugge, R., Fielding, M., & Fuentes, M. (2011). The ERA-Interim archive Version 2.0 Rep., 23 pp, ECMWF, Shinfield Park, Reading.
- Bevis, M., Businger, S., Chiswell, S., Herring, T. A., Anthes, R. A., Rocken, C., & Ware, R. H. (1994). GPS meteorology: Mapping zenith wet delays onto precipitable water. *Journal of Applied Meteorology*, 33(3), 379–386. [https://doi.org/10.1175/1520-0450\(1994\)033<0379:GMMZWD>2.0.CO;2](https://doi.org/10.1175/1520-0450(1994)033<0379:GMMZWD>2.0.CO;2)

Acknowledgments

We would like to thank the CNES/CLS for providing the satellite orbits and clocks, IGS and UNAVCO for the ground GNSS observations, ECMWF for the NWM, University of Wyoming for radiosonde data, and AVISO for the SARAL PWV. We are grateful to Marius Bratrein, Thomas Gerber, the crew and science team of the 2016 Fram Strait cruise for support during measurements. The ship-based GNSS measurements were realized in the ArGID (Arctic GNSS Ice Detection) project funded by GFZ. See <https://doi.pangaea.de/10.1594/PANGAEA.900131> for the ZTD and PWV data set. Jungang Wang and Zhilu Wu are financially supported by the China Scholarship Council (CSC, Files 201606260035 and 201706710115). This study is supported by National Natural Science Foundation of China (41876106) and Helmholtz Association (ADVANTAGE, ZT-0007).

- Boehm, J., Heinkelmann, R., & Schuh, H. (2007). Short note: A global model of pressure and temperature for geodetic applications. *Journal of Geodesy*, 81(10), 679–683. <https://doi.org/10.1007/s00190-007-0135-3>
- Boehm, J., Niell, A., Tregoning, P., & Schuh, H. (2006). Global mapping function (GMF): A new empirical mapping function based on numerical weather model data. *Geophysical Research Letters*, 33, L07304. <https://doi.org/10.1029/2005gl025546>
- Boniface, K., Champollion, C., Chery, J., Ducrocq, V., Rocken, C., Doerflinger, E., & Collard, P. (2012). Potential of shipborne GPS atmospheric delay data for prediction of Mediterranean intense weather events. *Atmospheric Science Letters*, 13(4), 250–256. <https://doi.org/10.1002/ASL.391>
- Brown, S. (2010). A novel near-land radiometer wet path-delay retrieval algorithm: Application to the Jason-2/OSTM Advanced Microwave Radiometer. *IEEE Transactions on Geoscience and Remote Sensing*, 48(4), 1986–1992. <https://doi.org/10.1109/tgrs.2009.2037220>
- Byun, S. H., & Bar-Sever, Y. E. (2009). A new type of troposphere zenith path delay product of the international GNSS service. *Journal of Geodesy*, 83(3–4), 1–7. <https://doi.org/10.1007/s00190-008-0288-8>
- Cardellach, E., Behrend, D., Ruffini, G., & Rius, A. (2000). The use of GPS buoys in the determination of oceanic variables. *Earth, Planets and Space*, 52(11), 1113–1116. <https://doi.org/10.1186/bf03352340>
- Chadwell, C. D., & Bock, Y. (2001). Direct estimation of absolute precipitable water in oceanic regions by GPS tracking of a coastal buoy. *Geophysical Research Letters*, 28(19), 3701–3704. <https://doi.org/10.1029/2001GL013280>
- de Steur, L., Hansen, E., Mauritzen, C., Beszczynska-Möller, A., & Fahrback, E. (2014). Impact of recirculation on the East Greenland Current in Fram Strait: Results from moored current meter measurements between 1997 and 2009. *Deep Sea Research Part I: Oceanographic Research Papers*, 92, 26–40. <https://doi.org/10.1016/j.jsr.2014.05.018>
- de Steur, L., Peralta-Ferriz, C., & Pavlova, O. (2018). Freshwater export in the East Greenland Current freshens the North Atlantic. *Geophysical Research Letters*, 45, 13,359–13,366. <https://doi.org/10.1029/2018GL080207>
- Dodson, A. H., Chen, W., Penna, N. T., & Baker, H. C. (2001). GPS estimation of atmospheric water vapour from a moving platform. *Journal of Atmospheric and Solar-Terrestrial Physics*, 63(12), 1331–1341. [https://doi.org/10.1016/s1364-6826\(00\)00251-0](https://doi.org/10.1016/s1364-6826(00)00251-0)
- Fernandes, M. J., Lazaro, C., Ablain, M., & Pires, N. (2015). Improved wet path delays for all ESA and reference altimetric missions. *Remote Sensing of Environment*, 169, 50–74. <https://doi.org/10.1016/j.rse.2015.07.023>
- Fernandes, M. J., Lazaro, C., Nunes, A. L., Pires, N., Bastos, L., & Mendes, V. B. (2010). GNSS-derived path delay: An approach to compute the wet tropospheric correction for coastal altimetry. *IEEE Geoscience and Remote Sensing Letters*, 7(3), 596–600. <https://doi.org/10.1109/LGRS.2010.2042425>
- Fujita, M., Kimura, F., Yoneyama, K., & Yoshizaki, M. (2008). Verification of precipitable water vapor estimated from shipborne GPS measurements. *Geophysical Research Letters*, 35, L13803. <https://doi.org/10.1029/2008GL033764>
- Gutman, S. I., Sahm, S. R., Benjamin, S. G., Schwartz, B. E., Holub, K. L., Stewart, J. Q., & Smith, T. L. (2004). Rapid retrieval and assimilation of ground based GPS precipitable water observations at the NOAA Forecast Systems Laboratory: Impact on weather forecasts. *Journal of the Meteorological Society of Japan*, 82(1B), 351–360. <https://doi.org/10.2151/JMSJ.2004.351>
- Kealy, J., Foster, J., & Businger, S. (2012). GPS meteorology: An investigation of ocean-based precipitable water estimates. *Journal of Geophysical Research*, 117, D17303. <https://doi.org/10.1029/2011JD017422>
- Li, X., Zus, F., Lu, C., Dick, G., Ning, T., Ge, M., et al. (2015). Retrieving of atmospheric parameters from multi-GNSS in real time: Validation with water vapor radiometer and numerical weather model. *Journal of Geophysical Research: Atmospheres*, 120, 7189–7204. <https://doi.org/10.1002/2015JD023454>
- Liu, J., & Ge, M. (2003). PANDA software and its preliminary result of positioning and orbit determination. *Wuhan University Journal of Natural Sciences*, 8(2), 603–609. <https://doi.org/10.1007/BF02899825>
- Loyer, S., Perosanz, F., Mercier, F., Capdeville, H., & Mezerette, A. (2016). CNES/CLS IGS Analysis Center: Contribution to MGEX and recent activities, in IGS Workshop 2016. Sydney, Australia.
- Mahesh Kumar, U., Sasamal, S. K., Swain, D., Narendra Reddy, N., & Ramanappa, T. (2015). Intercomparison of Geophysical Parameters From SARAL/AltiKa and Jason-2 Altimeters. *IEEE Journal of Selected Topics in Applied Earth Observations and Remote Sensing*, 8(10), 4863–4870. <https://doi.org/10.1109/JSTARS.2015.2469757>
- Oigawa, M., Tsuda, T., Seko, H., Shoji, Y., & Realini, E. (2018). Data assimilation experiment of precipitable water vapor observed by a hyper-dense GNSS receiver network using a nested NHM-LETKF system. *Earth, Planets and Space*, 70(1). <https://doi.org/10.1186/s40623-018-0851-3>
- Penna, N. T., Morales Maqueda, M. A., Martin, I., Guo, J., & Foden, P. R. (2018). Sea surface height measurement using a GNSS wave glider. *Geophysical Research Letters*, 45(11), 5609–5616. <https://doi.org/10.1029/2018gl077950>
- Picard, B., Frery, M. L., Obligis, E., Eymard, L., Steunou, N., & Picot, N. (2015). SARAL/AltiKa wet tropospheric correction: In-flight calibration, retrieval strategies and performances. *Marine Geodesy*, 38(sup1), 277–296. <https://doi.org/10.1080/01490419.2015.1040903>
- Renner, A. H. H., Gerland, S., Haas, C., Spreen, G., Beckers, J. F., Hansen, E., et al. (2014). Evidence of Arctic sea ice thinning from direct observations. *Geophysical Research Letters*, 41, 5029–5036. <https://doi.org/10.1002/2014GL060369>
- Rocken, C., Johnson, J., Van Hove, T., & Iwabuchi, T. (2005). Atmospheric water vapor and geoid measurements in the open ocean with GPS. *Geophysical Research Letters*, 32, L12813. <https://doi.org/10.1029/2005GL022573>
- Saastamoinen, J. (1972). Atmospheric correction for the troposphere and stratosphere in radio ranging satellites. In S. W. Henriksen, A. Mancini, & B. H. Chovitz (Eds.), *The use of artificial satellites for geodesy* (pp. 247–251). Washington DC: American Geophysical Union. <https://doi.org/10.1029/GM015P0247>
- Semmling, A. M., Rösel, A., Ludwig, M., Bratrein, M., Gerland, S., & Wickert, J. (2017). A Fram Strait Experiment: Sensing sea ice conditions using shipborne GNSS reflectometry, in 19th EGU General Assembly 2017. Vienna, Austria.
- Verron, J., Sengenès, P., Lambin, J., Noubel, J., Steunou, N., Guillot, A., et al. (2015). The SARAL/AltiKa altimetry satellite mission. *Marine Geodesy*, 38(sup1), 2–21. <https://doi.org/10.1080/01490419.2014.1000471>
- Wang, J., Zhang, L., & Dai, A. (2005). Global estimates of water-vapor-weighted mean temperature of the atmosphere for GPS applications. *Journal of Geophysical Research*, 110, D21101. <https://doi.org/10.1029/2005JD006215>
- Wang, J., Zhang, L., Dai, A., Van Hove, T., & Van Baelen, J. (2007). A near-global, 2-hourly data set of atmospheric precipitable water from ground-based GPS measurements. *Journal of Geophysical Research*, 112, D11107. <https://doi.org/10.1029/2006JD007529>
- Zus, F., Bender, M., Deng, Z. G., Dick, G., Heise, S., Shang-Guan, M., & Wickert, J. (2012). A methodology to compute GPS slant total delays in a numerical weather model. *Radio Science*, 47, RS2018. <https://doi.org/10.1029/2011rs004853>